4-3-2015

Characterization of a soft elastomeric capacitive strain sensor for fatigue crack monitoring

Xiangxiong Kong
University of Kansas

Jian Li
University of Kansas

Simon Laflamme
Iowa State University, laflamme@iastate.edu

Caroline Bennett
University of Kansas

Adolfo Matamoros
University of Texas at San Antonio

Characterization of a soft elastomeric capacitive strain sensor for fatigue crack monitoring

Abstract
Fatigue cracks have been one of the major factors for the deterioration of steel bridges. In order to maintain structural integrity, monitoring fatigue crack activities such as crack initiation and propagation is critical to prevent catastrophic failure of steel bridges due to the accumulation of fatigue damage. Measuring the strain change under cracking is an effective way of monitoring fatigue cracks. However, traditional strain sensors such as metal foil gauges are not able to capture crack development due to their small size, limited measurement range, and high failure rate under harsh environmental conditions. Recently, a newly developed soft elastomeric capacitive sensor has great promise to overcome these limitations. In this paper, crack detection capability of the capacitive sensor is demonstrated through Finite Element (FE) analysis. A nonlinear FE model of a standard ASTM compact tension specimen is created which is calibrated to experimental data to simulate its response under fatigue loading, with the goal to 1) depict the strain distribution of the specimen under the large area covered by the capacitive sensor due to cracking; 2) characterize the relationship between capacitance change and crack width; 3) quantify the minimum required resolution of data acquisition system for detecting the fatigue cracks. The minimum resolution serves as a basis for the development of a dedicated wireless data acquisition system for the capacitive strain sensor.

Keywords
Fatigue crack, crack detection, capacitive sensor, structural health monitoring, compact tension specimen

Comments
This proceeding is published as Xiangxiong Kong, Jian Li, Simon Laflamme, Caroline Bennett, Adolfo Matamoros, "Characterization of a soft elastomeric capacitive strain sensor for fatigue crack monitoring", Proc. SPIE 9435, Sensors and Smart Structures Technologies for Civil, Mechanical, and Aerospace Systems 2015, 94353I (3 April 2015); doi: 10.1117/12.2176631. Posted with permission.

Characterization of a soft elastomeric capacitive strain sensor for fatigue crack monitoring

Xiangxiong Kong [a], Jian Li [a*], Simon Laflamme [b,c], Caroline Bennett [a], and Adolfo Matamoros [d]

[a]Department of Civil, Environmental and Architectural Engineering,
University of Kansas, Lawrence, KS 66045, USA
[b]Department of Civil, Construction, and Environmental Engineering,
Iowa State University, Ames, IA, 50011, USA
[c]Department of Electrical and Computer Engineering,
Iowa State University, Ames, IA, 50011, USA
[d]Department of Civil and Environmental Engineering,
University of Texas at San Antonio, San Antonio, TX, 78249, USA

ABSTRACT

Monitoring the initiation and propagation of fatigue cracks is one of the primary concerns of bridge engineers in charge of overseeing the condition of structural steel bridges. Given the scarcity of resources available for bridge maintenance, engineers are often forced to prioritize bridge rehabilitation projects, and in many instances have to rely on monitoring fatigue crack growth to make sure that there is no threat to structural integrity while bridges remain in service. Measuring the deformation in the area surrounding fatigue cracks has been shown to be an effective way of monitoring the rate of crack growth. Traditional strain sensors such as metal foil gauges have a limited ability to capture crack initiation and growth due to their small size, limited measurement range, and high failure rate under harsh environmental conditions. Recently, a newly developed soft elastomeric capacitive sensor has shown great promise to overcome these limitations and tests have demonstrated its capability to detect fatigue cracks. In this paper, the crack detection capability of the capacitive sensor is validated through Finite Element (FE) analysis. A nonlinear FE model of a standard ASTM compact tension specimen was created and calibrated using experimental data to simulate its response under fatigue loading, with the objectives of: 1) depicting the strain distribution of the specimen due to cracking under the large area covered by the capacitive sensor; 2) characterize the relationship between capacitance change measured by the SEC sensor and crack width. This relationship facilitates quantitative evaluation of crack development using the newly developed SEC sensor.

Keywords: Fatigue crack; crack detection; capacitive sensor; structural health monitoring, compact tension specimen.

1. INTRODUCTION

Fatigue-induced cracks are a major source of damage in steel bridges. In particular, fracture critical bridges are of most concern because the rapid propagation of cracks can result in a brittle and sudden failure. Detecting these cracks, especially at an early stage of growth, is still a very challenging problem[1]. By far the most common method for detecting fatigue cracks is visual inspection. Some disadvantages of this approach are that it is time consuming, labor intensive, cost inefficient, and prone to error due to how difficult it is to consistently identify the location of the tip of the crack. Although nondestructive evaluation techniques can improve the accuracy of inspection [2], [3], the lack of autonomy and continuity in the inspection process limits the ability to measure the rate of crack growth in a timely manner. Fatigue cracks may also develop between scheduled inspection dates and can go undetected before a catastrophic failure occurs.

Various techniques for crack detection in structures have been studied in the past. Park et al. [4] applied piezoelectric lead-zirconate–titanate (PZT) patch sensors to detect crack growth in a reduced-scale steel bridge component. Ihn [5] [6] applied a similar technique to monitor crack growth in a metallic aircraft structure. Roberts [7] used an acoustic emission

*Assistant Professor; Email: jianli@ku.edu

Sensors and Smart Structures Technologies for Civil, Mechanical, and Aerospace Systems 2015,
edited by Jerome P. Lynch, Kon-Well Wang, Hoon Sohn, Proc. of SPIE Vol. 9435, 94353I
 · doi: 10.1117/12.2176631

system to monitor fatigue crack growth in a compact tension steel plate and a T-section girder component. Mi [8] applied ultrasonic sensors to detect initiation and growth of fatigue cracks in an aluminum beam based on the relationship between the ultrasonic signal and the applied load. The main disadvantage of piezoelectric or ultrasonic sensors is that they require an actuator to generate the signals, which raises concerns about high power consumption and increases the complexity of the design of the monitoring system. Measuring the average strain over a finite area has been shown to be effective in detecting crack growth. Kamaya [9] [10] performed a feasibility study for monitoring the internal crack growth of a metallic specimen by measuring the external variation in strain. Typical metal foil strain gauges have relatively small size and are limited to detecting cracks in the immediate proximity of the sensor. Moreover, their limited measurement range and ductility leads to failure of the sensor when a crack occurs. A comprehensive review on crack detection techniques can be found in Yao et al. [1]

In a recent study, a soft elastomeric capacitor (SEC) sensor [11] showed great promise for monitoring crack growth through strain measurement. When attached to structural surfaces, this SEC sensor converts surface strains into capacitance changes. Compared with traditional metal foil strain gauges, the SEC sensor can occupy a much larger size and has greater ductility, making it better suited for monitoring crack growth over a larger area than metal foil gages. The accuracy of strain measurements obtained using the SEC sensor was verified through [12] a beam bending test in which the sensor was subjected to unidirectional strains. Kharroub et al. [13] performed a preliminary investigation on the crack detection capability of the SEC sensor based on a series of low-cycle fatigue tests of compact tension steel specimens. These tests showed that the SEC sensor can be used effectively to detect and localize fatigue cracks. Although the capacitance changes were recorded continuously during the fatigue tests, it was not possible to establish a correlation between crack length and the measured capacitance change because crack length was recorded only at the end of the tests.

The crack detection capability of the SEC sensor is validated in this paper through Finite Element (FE) analysis. A nonlinear FE model of the compact tension specimen tested by Kharroub et al. [13] was developed based on the dimensions and material properties of the test specimens, and calibrated using experimental data to simulate the response of the specimen to fatigue loading. The change in the area covered by the SEC sensor was used to calculate the change in capacitance, and to establish a relationship between capacitance change and crack width needed to calibrate the SEC sensor. The main objectives of the simulations were: 1) to map the strain distribution under the area covered by the SEC sensor as the crack propagated; 2) to characterize the relationship between capacitance change and crack width.

2. SOFT ELASTOMERIC CAPACITOR AND CRACK DETECTION TESTS

The equations for converting capacitance measurements into strains presented in the following are only applicable to the elastic deformation of an SEC subjected to in-plane stress. After the crack has occurred, the deformation of the SEC is highly localized and most likely beyond the proportional limit of the material, so the equations constitute only an approximation.

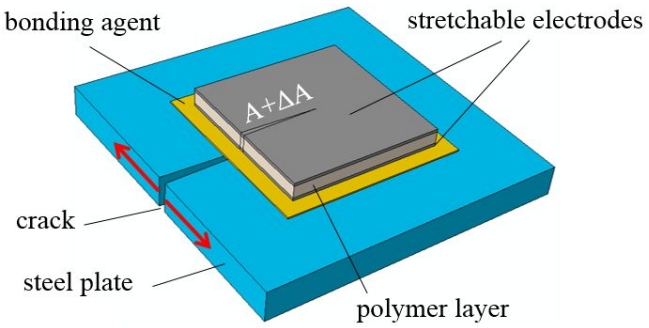

Figure 1. Schematic of the SEC sensor

2.1 Soft elastomeric capacitor

The sensing principle of the SEC sensor is illustrated in Fig. 1. The SEC sensor is comprised of a three-layer structure in which the top and bottom layers are compliant electrodes. These electrodes move simultaneously with structural surface under strain. The middle layer is the dielectric. As shown in Figure 1, after a crack occurs in the structural component, the geometry change of the SEC sensor leads to a change in its electrical properties, which can be measured as a change in capacitance using a data acquisition (DAQ) system. More details of the SEC sensor can be found in reference [11].

The SEC can be modeled as a non-lossy capacitor under low measurement frequencies (< 1 kHz):

$$C = \frac{e_0 e_r A}{h} \tag{1}$$

where C is the capacitance of the SEC sensor, $e_0 = 8.854$ pF/m is the vacuum permittivity, e_r is the relative permittivity of the polymer, and A and h are the area and thickness of the effective dielectric. A positive strain induced by a crack (Figure 1) leads to an increased area A and a decreased thickness h due to Poisson's effect, and results in a higher capacitance of the SEC sensor.

An electromechanical model has been derived in [11] using Eq. (1) and Hooke's Law for in-plane stresses:

$$\frac{\Delta C}{C} = \frac{1}{1-\nu}\left(\varepsilon_x + \varepsilon_y\right) \tag{2}$$

where ΔC is the change in capacitance, and ε_x and ε_y are the strains along the in-plane axes x and y, respectively, and ν is Poisson's ratio of the SEC material, taken as $\nu \approx 0.49$. The resulting gauge factor of the SEC is $\lambda = 1/1-\nu \approx 2$. The accuracy of strain measurement using the SEC sensor was validated through a bending beam test. [12] In the case of bi-directional strain, the capacitance change is a result of the additive strains in both directions as shown in Eq. (2).[13]

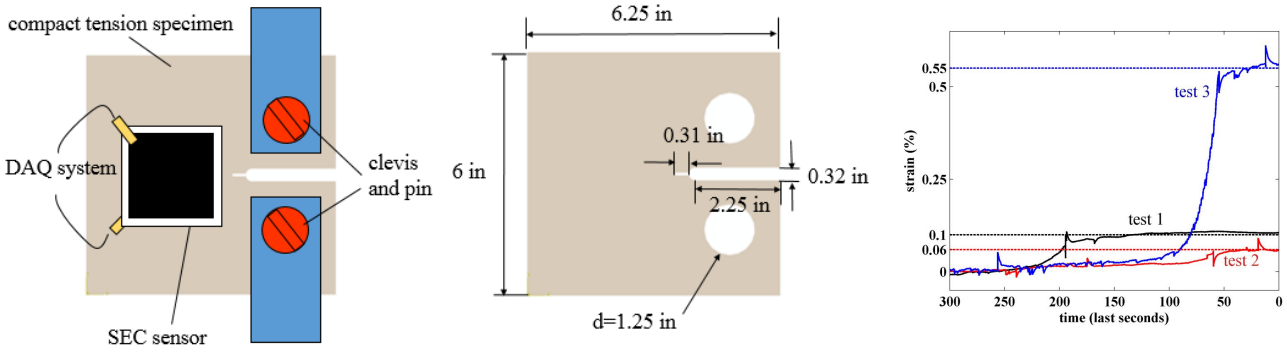

(a) (b) (c)

Figure 2. (a) Schematic of the test setup; (b) dimensions of the test specimens; (c) measured capacitance change vs. time in three tests

2.2 Crack detection tests

To evaluate the crack detection capability of the SEC sensor, a series of low-cycle fatigue tests using ASTM E647-13a compact tension (CT) specimens were performed [13]. The specimens, made of A36 steel with a tensile strength of 72.5 ksi, had rectangular shape with two punched holes. A horizontal notch with a length of 2.25 in. was fabricated between the two holes. The specimens were cut to a length 0.31 in. at the tip of the notch to facilitate the growth of fatigue cracks. A tensile cyclic loading with a maximum of 6.5 kips and a minimum of 0.65 kips was applied to the specimens through the clevis and pins attached to the two holes, as shown in Fig. 2a. The loading frequency was 20 Hz. An SEC sensor with

a size of 2.64 × 2.64 in. was is attached to one side of the specimens and was connected to a DAQ system to measure capacitance change. A schematic of the test configuration is shown in Fig. 2a and the dimensions of the test specimens are shown in Fig. 2b.

Three specimens were tested. The results showed that at the end of the tests the total crack length measured for the three specimens reached 1.18 in., 1.61 in. and 1.28. in., respectively. The crack widths at the end of the tests were 0.01 in., 0.012 in. and 0.03 in., respectively. The crack lengths and widths were measured by a pixel count from pictures taken using a using a Canon T2i DSLR camera 18.0-megapixel. Fig. 2c shows the total measured strain $\varepsilon_x+\varepsilon_y$ using Eq. (2) and a gauge factor λ=2. As shown in Fig. 2c, the measured capacitance values of the SEC sensors increased significantly after the cracks occurred.

3. FINITE ELEMENT MODEL

While the crack detection capability of the SEC sensors was experimentally demonstrated, due to the limitations imposed by the test configuration, the crack width and length were only measured at the end of each test. As a result, the measured relationship between the capacitance of the sensor and the crack size is not available. In this section, an FE model developed using the commercially-available program Abaqus (version 6.13) was used to simulate the experiment to quantify the relationship between crack size and capacitance response of the sensor. An element removal algorithm was adopted in the analysis to simulate the crack propagation process. The most significant characteristics of the FE model such as the type of material model, mesh distribution, capacitance calculation for the SEC sensor based on the simulated plate deformation, and the calibration of the crack element size are discussed in the following.

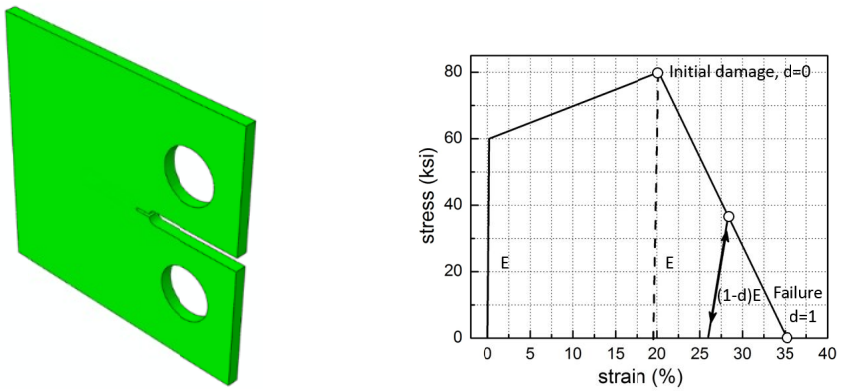

Figure 3. (a) Schematic of the FE model; (b) strain and stress relationship of material

3.1 Crack propagation simulation

Simulating crack propagation is a challenging task because of the highly nonlinear behavior in the vicinity of the tip of the crack. The first author of this paper had applied an approach based on a material failure theory and an element removal technique in simulating progressive collapse of a steel structure [14]. This approach does not require a pre-defined crack direction before analysis and is adopted herein to simulate crack propagation.

The nonlinear stress-strain relationship of the material adopted in the FE model is shown in Figure 3b. The material model was intended to represent the most important characteristics of the A36 steel used for the specimens. Young's modulus of the material was 29,000 ksi and Poisson's ratio was 0.26. The yield strength and tensile strength of A36 steel were defined considering the uncertainties reported in the literature. A statistical data analysis in FEMA 267 [15] demonstrated that the A36 steel normally reaches a yield stress from 36 ksi to 72.4 ksi, and the tensile strength is between 68.5 ksi and 88.5 ksi. Similarly, ASTM A36 [16] considered 36 ksi as the lower limit of yield strength and 50 ksi to 80 ksi as the required tensile strength range for A36 steel. Furthermore, a statistical analysis [17] based on 4,225 test results showed that the actual tested values of yield and tensile strength in steel product were 10% larger than the nominal yield and tensile strength, respectively. In this study, the tensile strength of the material is defined as 80 ksi. The

yield strength, on the other hand, is defined as 60 ksi, which satisfies the required lower limit of 36 ksi and is within the range reported in FEMA 267 [15].

Beyond the tensile strength of 80 ksi, material damage accumulates until complete failure. A damage variable *d* was introduced to control stiffness degradation, by which element failure is defined. The element was removed when failure occurred. As shown in Figure 3b, the damage variable *d* equals 0 at the initial damage point. With the increase of plastic strain, *d* increased linearly, resulting in a reduction of the unloading stiffness. When *d* reached 1.0, the failure element was removed automatically [18] and no longer existed in the FE model. A series of element removals simulated the crack propagation process as material failed due to excessive plastic strain developed by cracking.

3.2 Mesh distribution

The overall dimensions of the FE model were the same as the specimen shown in Fig. 2b. Three-dimensional shell elements with a thickness of 0.25 in. were used to model the steel plate. The schematic of the FE model is shown in Figure 3a.

The FE model was meshed considering three factors. First, as shown in Fig. 4b, the region with the potential for elements to be removed due to crack propagation was modeled with small-size elements. The tight mesh density for these likely-to-crack elements was defined based on test data, as discussed in Section 3.4. Outside of this region, the element size increased and reached 0.1 in. × 0.1 in. at the edges of the specimen. Second, a square area shown in Fig. 4a with the size of the SEC sensor (2.64 in. × 2.64 in.) was meshed separately to simulate the response of the SEC sensor during testing. The SEC sensor attached to the specimen was not included in the model due to its relatively small stiffness (its thickness was approximately 0.01 in.). Instead, the capacitance of the SEC sensor was calculated based on the change in surface area computed in these elements, based on the assumption of perfect bond between the sensor and the specimen. Finally, the remainder of the specimen was meshed with similar-size elements as in the sensor area. The mesh distribution and the configuration of the model around the tip of the notch are shown in Figure 4a and 4b, respectively.

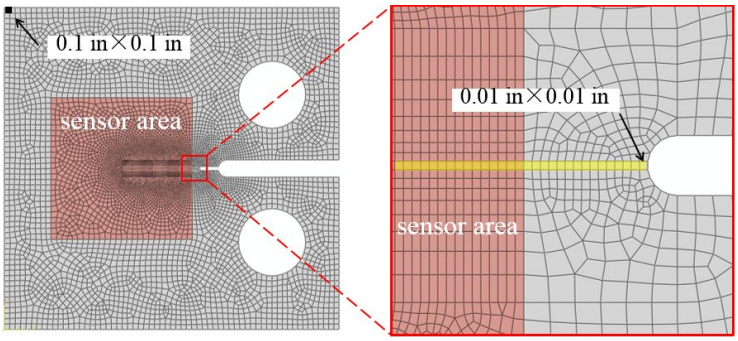

Figure 4. (a) FE model; (b) configuration of the model near the tip of the notch

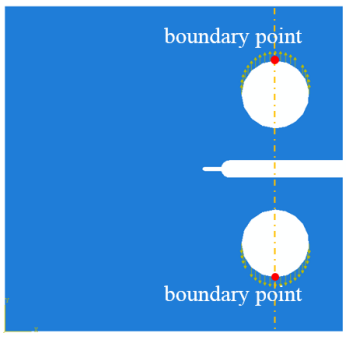

Figure 5. Boundary conditions

3.3 Loads and boundary conditions

In the physical simulations cyclic loading was applied in the vertical direction through pins attached to the holes in the specimens. In the FE model, distributed tension loads were applied at the upper half of the top hole and the lower half of the bottom hole (Figure 5) to simulate the cyclic loading applied to the specimens. The maximum and minimum amplitude of the cyclic loading were 6.5 kips and 0.65 kips, respectively. The loading amplitudes were selected to yield a meaningful rate of crack growth. Horizontal motion of the model was constrained at the two boundary points as shown in Fig. 5.

3.4 Simulated capacitance measurement of the SEC sensor

As mentioned in Section 3.2, the SEC sensor used in the experiment was not included in the computational model due to its small thickness. Instead, the capacitance of the SEC sensor was calculated based on the simulated response of the shell elements within the area occupied by the sensor in the FE model. The capacitance change in the SEC sensor

corresponding to each individual element under the sensor area was calculated based on the simulated bi-directional strains using Eq. (2), assuming that each element within the area covered by the sensor experienced a uniform strain field. A simpler approach is presented herein which does not require the extraction of bi-direction strains from the simulation results. Instead, it relies on the area of each element before and after deformation which simplifies the process of converting the results from the FE model into the capacitance change of the SEC sensor.

Based on Eq. (1), C_0 and C_1 are the capacitance values of the SEC sensor before and after deformation, respectively. The ratio of the change of capacitance due to the deformation in the area covered by the sensor can be expressed as

$$\frac{\Delta C}{C_0} = \frac{C_1 - C_0}{C_0} = \frac{e_0 e_r (\frac{A_1}{h_1} - \frac{A_0}{h_0})}{e_0 e_r \frac{A_0}{h_0}} = \frac{A_1 h_0}{A_0 h_1} - 1 \tag{3}$$

where A_0 and h_0 are the initial area and thickness of the SEC sensor, respectively, and A_1 and h_1 are the deformed area and thickness, respectively. Based on the assumption that the sensor material is incompressible [12], i.e., the volume is constant before and after deformation, the initial thickness of the SEC sensor can be expressed as

$$h_0 = \frac{A_1 h_1}{A_0} \tag{4}$$

Substituting Eq. (4) into Eq. (3), a relationship between the change in capacitance and the change in area is obtained as

$$\frac{\Delta C}{C_0} = \frac{A_1^2}{A_0^2} - 1 \tag{5}$$

The FE model used in this study had a total of 7,102 elements in the area covered by the sensor. For a single element, *i*, assuming that the strain field is uniform within the element, the capacitance change can be expressed as

$$\frac{\Delta C_i}{C_{0i}} = (\frac{A_{1i}^2}{A_{0i}^2} - 1) \tag{6}$$

Note that the initial capacitance C_{0i} for element *i* is proportional to the area of that element, i.e.

$$C_{0i} = \frac{A_{0i}}{A_0} C_0 \tag{7}$$

Substituting Eq. (7) into Eq. (6), the capacitance change of element *i* is obtained as

$$\Delta C_i = \frac{A_{0i}}{A_0} C_0 (\frac{A_{1i}^2}{A_{0i}^2} - 1) \tag{8}$$

The total capacitance change of the whole sensor can be calculated as the sum of the capacitance changes for all of the 7,102 elements under the sensor:

$$\Delta C = \sum_{i=1}^{7102} \Delta C_i = \frac{C_0}{A_0} \sum_{i=1}^{7102} A_{0i} (\frac{A_{1i}^2}{A_{0i}^2} - 1) \tag{9}$$

Finally, the capacitance change ratio of the SEC sensor can be expressed as

$$\frac{\Delta C}{C_0} = \frac{1}{A_0} \sum_{i=1}^{7102} A_{0i} (\frac{A_{1i}^2}{A_{0i}^2} - 1) \tag{10}$$

3.4 Element size in the crack region

As shown in Eq. (10), the capacitance change is a function of the initial and the deformed areas of each element. For elements that are not located along the path of the crack, these two areas can be easily extracted from the simulation results. In the simulation technique used, as the crack propagated, the elements along the path of the crack were removed from the FE model. This is different from the behavior of the SEC sensor attached to the physical specimen in that the sensor did not crack and covered the opened crack region of the specimen. Compatibility dictates that the deformed area of the removed elements must increase in proportion to the width of the opened crack. Because the size of the elements in the path of the crack significantly affects the accuracy of the calculated capacitance change of the sensor, the size of the elements in this region of the mesh was selected such that the calculated change in capacitance would match the experimental results.

During the tests it was observed that the SEC sensor did not crack when the crack propagated directly underneath it. This behavior is attributed to the high ductility of the sensor and to localized slippage between the sensor and the specimen in the vicinity of the crack. As the crack propagated in the computational model, removed elements had the effect of smearing the localized deformation of the sensor material in the crack region over a finite element width that depended on the configuration of the mesh. The outcome of this modeling approach was that instead of simulating a highly localized deformation that can cause breakage of the sensor, the average strain demand was computed over the area of the elements and the calculated demand on the material was much lower than in the test. Since accurately simulating the local effects of slippage and sensor yielding in the region over a crack is a very difficult task, defining the size of the elements in this region of the mesh was essential to being able to match the capacitance values measured in the tests. In this study, the size of the crack elements was used to calibrate the FE model such that the capacitance response matched the test results for different crack sizes. The final size of the elements in the path of the crack was selected as 0.01 in × 0.01 in.

4. SIMULATION RESULTS AND DISCUSSION

4.1 Simulated crack propagation and strain distribution

The progression of the crack under the low-cycle fatigue loading was simulated using the FE model. At the beginning of loading, the element located at the tip of the pre-notched section (marked with highlighted yellow color in Fig. 4b experienced plastic deformations due to the high strain demand induced by the notch, which led to an accumulation of damage in that element. This element was considered to have failed and was removed after the damage variable *d* reached 1. After the initial loading step, elements were sequentially removed based on the strain demand as the cyclic loading proceeded. Figures 6a to 6c show the simulated progression of the crack. The deformation scale factors in the figures were set to 1.0 to display a realistic deformed amplitude of the FE model. The final deformed configuration of one of the test specimens is shown in Fig. 6d for comparison. The comparison indicates the FE model had a similar crack pattern as the test specimen.

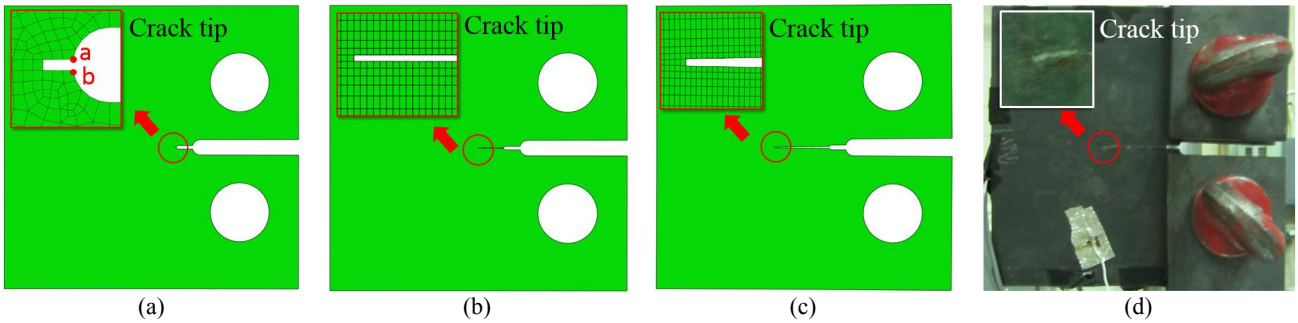

(a) (b) (c) (d)

Figure 6. Simulated crack progression: (a) crack length = 0.03 in; (b) crack length = 0.53 in; (c) crack length = 1.17 in; (d) test specimen

Changes in the strain field due to crack propagation were also investigated based on the simulation results. Figure 7 shows the Equivalent Plastic Strain (PEEQ) computed with the FE model as the crack progressed. The results indicate that, as expected, the maximum strain consistently occurred at the tip of the crack. The calculated strain was less than the failure point defined in Figure 3b, which was 35% in this case. The results also showed that calculated strain was very highly localized in the vicinity of the tip of the crack, while the remainder of the FE model remained in the elastic range. This localized strain demand indicates that the SEC sensor would perform best for crack detection if it were located over the crack, and that an SEC sensor located far away from the path of crack propagation would not generate a significant change in capacitance. This limitation also applies to traditional metal film strain gauges, although the SEC sensor evaluated in this study has a much larger size and has a higher probability of capturing crack initiation or crack propagation than metal film strain gages when deployed on structural surfaces.

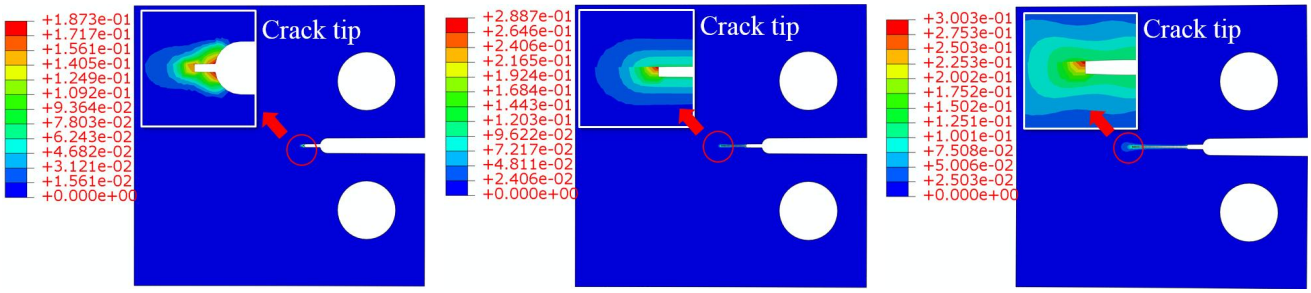

(a) (b) (c)

Figure 7. Strain distribution during crack propagation: (a) crack length = 0.03 in.; (b) crack length = 0.53 in.; (c) crack length = 1.17 in

4.2 Verification of simulation results

The advantage of the FE analyses performed in this study is that the complete relationship between crack size and capacitance change during loading could be obtained, whereas only one data point was available for each experimental test. The capacitance change ratio was plotted against the crack width for both FE analysis and the tests in Fig. 8. Crack width was selected to characterize crack size because larger uncertainty was observed in the measured crack length, and because crack width had a better correlation with the measured capacitance change. The simulated crack width presented in Fig. 8a was obtained by measuring the relative vertical distance between point *a* and *b* as shown in Fig. 6a.

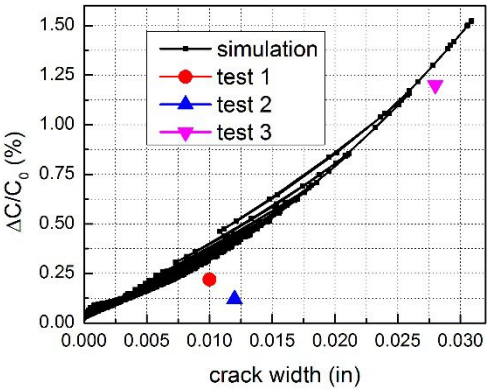

Figure 8. Capacitance response vs. crack width

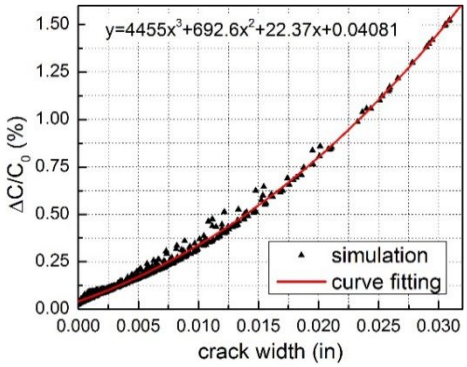

Figure 9. Linear regression results for the relationship between change in capacitance and crack width;

A nonlinear relationship was observed between the change in capacitance and crack width (Fig. 8a). The observed trend was similar for the simulation results and the test data, which indicates that the FE model can be used to simulate the crack progression of the test specimen accurately. Furthermore, the results also indicate that the equation for computing capacitance change presented in Section 2.2 of this paper used in combination with the FE model gave reliable estimates

of the change in capacitance due to crack propagation, even though the crack generates a complicated non-uniform bi-directional strain field in the SEC sensor.

Based on the simulated data points shown in Fig. 8, regression analyses were performed to investigate the relationship between the capacitance change and crack width. For the particular test specimen investigated in this study, a third order polynomial function was found to provide an accurate representation of this relationship. Similar relationships can be obtained for other types of structures to facilitate quantitative crack monitoring based on capacitance measurement using the SEC sensor.

CONCLUSIONS

In this paper, the use of an SEC sensor to monitor fatigue crack propagation in steel structures was evaluated. To facilitate quantitative crack monitoring, an FE model developed using ABAQUS was used to simulate the crack propagation observed in a test specimen subjected to low-cycle fatigue loading. Crack propagation was simulated through the combined implementation of a damage theory for the specimen material and an element removal algorithm. As material damage accumulated due to cyclic loading, failed elements were removed from the FE model when a damage threshold was exceeded. The SEC sensor was not included in the FE model due to its small thickness. Instead, the change in capacitance of the SEC sensor was simulated on the basis of the change in area of the elements within the region covered by the sensor. Element size along the path of crack propagation was calibrated based on test data. The simulation results showed that, as expected, there was a highly non-uniform and localized strain field in the vicinity of the tip of the crack. For this reason crack detection based on strain measurements is only effective when a crack initiates in the vicinity of or directly underneath the strain sensor. The large footprint of the SEC sensor makes it a better solution than traditional metal foil gauges. A comparison between simulation and test results shows that the FE model was able to represent accurately the relationship between capacitance change and crack width. The approach proposed in this study can be applied to other structures to quantify the relationship between crack size and capacitance change in order to facilitate crack size monitoring using the SEC sensor.

ACKNOWLEDGEMENTS

This work was supported by the Iowa Department of Transportation grant #RT454-494 and the Kansas Department of Transportation. Their support is gratefully acknowledged.

REFERENCE

[1] Yao, Y., Tung, S. T. E., & Glisic, B., “Crack detection and characterization techniques — An overview,” Structural Control and Health Monitoring, 21(12), 1387-1413 (2014).
[2] Altschuler, E., & Pignotti,, “A Nonlinear model of flaw detection in steel pipes by magnetic flux leakage,” NDT & E International, 28(1), 35-40 (1995).
[3] Walle, G., & Netzelmann, U., “Thermographic crack detection in ferritic steel components using inductive heating,” Proceedings of the Ninth ECNDT, Berlin, Germany, Sept, 25-29 (2006).
[4] Park, S., Yun, C. B., Roh, Y., & Lee, J. J., “PZT-based active damage detection techniques for steel bridge components,” Smart Materials and Structures. 15(4), 957 (2006).
[5] Ihn, J. B., & Chang, F. K., “Detection and monitoring of hidden fatigue crack growth using a built-in piezoelectric sensor/actuator network: I. Diagnostics,” Smart Materials and Structures. 13(3), 609 (2004).
[6] Ihn, J. B., & Chang, F. K.,” Detection and monitoring of hidden fatigue crack growth using a built-in piezoelectric sensor/actuator network: II. Validation using riveted joints and repair patches,” Smart Materials and Structures. 13(3), 621 (2004).
[7] Roberts, T., & Talebzadeh, M., “Acoustic emission monitoring of fatigue crack propagation,” Journal of Constructional Steel Research. 59(6), 695-712 (2003).
[8] Mi, B., Michaels, J. E., & Michaels, T. E., “An ultrasonic method for dynamic monitoring of fatigue crack initiation and growth,” The Journal of the Acoustical Society of America. 119(1), 74-85 (2006).

[9] Kamaya, M., & Miyoshi, K., “Monitoring of inside surface crack growth by strain measurement of the outside surface: a feasibility study,” Nuclear Engineering and Design. 241(1), 1-11 (2011).
[10] Kamaya, M., “Monitoring of inside surface crack growth by strain measurements of the outside surface: Application of multiple strain measurements technique to fatigue crack growth,” Nuclear Engineering and Design. 256, 202-213 (2013).
[11] Laflamme, S., Kollosche, M., Connor, J. J., & Kofod, G., “Robust flexible capacitive surface sensor for structural health monitoring applications,” Journal of Engineering Mechanics. 139(7), 879-885 (2012).
[12] Laflamme, S., Saleem, H. S., Vasan, B. K., Geiger, R. L., Chen, D., Kessler, M. R., & Rajan, K., “Soft Elastomeric Capacitor Network for Strain Sensing Over Large Surfaces,” Mechatronics, IEEE/ASME Transactions on, 18(6), 1647-1654 (2013).
[13] Kharroub, S., Laflamme, S., Song, C., Qiao, D., Phares, B., Li, J., “Smart Sensing Skin for Detection and Localization of Fatigue Cracks,” Smart Materials and Structures, in press (2015).
[14] Kong, X., Shi, T., Cheng, S., “A numerical simulation method for steel structure collapsing under rare earthquakebase on the material damage and failure law,” China Civil Engineering Journal. 47(9), 38-44 (2014).
[15] Applied Technology Council, [Interim guidelines: evaluation, repair, modification and design of steel moment frames], FEMA-267, Rep. No. SAC-95-02, Federal Emergency Management Agency (1995).
[16] American Society for Testing and Materials, [Standard Specification for Carbon Structural Steel], ASTM A36, ASTM International, (2012).
[17] Rang, T., Yu, W., Galambos, T., "Load and resistance factor design of cold-formed steel statistical analysis of mechanical properties and thickness of materials combined with calibrations of the AISI design provisions of unstiffened compression elements and connections," Center for Cold-Formed Steel Structures Library. Paper 32. (1979).
[18] Hibbett, Karlsson, & Sorensen. [ABAQUS/standard: User's Manual (Vol. 1)], Hibbitt, Karlsson & Sorensen (1998).